

Article

Study on the Compatibility of Eco-Friendly Insulating Gas $C_5F_{10}O/N_2$ and $C_5F_{10}O/Air$ with Copper Materials in Gas-Insulated Switchgears

Yalong Li ¹, Xiaoxing Zhang ^{1,2,3,*} , Yalong Xia ^{4,*}, Yi Li ¹ , Zhuo Wei ¹, Yi Wang ²  and Song Xiao ¹

¹ School of Electrical Engineering and Automation, Wuhan University, Wuhan 430072, China; yalongli1122@whu.edu.cn (Y.L.); liyi_whuee@163.com (Y.L.); Sagittarius_weiz@163.com (Z.W.); xiaosongxs@gmail.com (S.X.)

² Hubei Key Laboratory for High-efficiency Utilization of Solar Energy and Operation Control of Energy Storage System, Hubei University of Technology, Wuhan 430068, China; 15927079934@163.com

³ State Key Laboratory of Power Transmission Equipment & System Security and New Technology, Chongqing University, Chongqing 400044, China

⁴ State Grid Sichuan Electric Power Research Institute, Chengdu 610000, China

* Correspondence: xiaoxing.zhang@outlook.com (X.Z.); xia.yalong@163.com (Y.X.)

Abstract: Sulfur hexafluoride (SF_6) is widely used in the power industry because of its excellent insulation and arc extinguishing performance. However, the high greenhouse effect of this material is being restricted by many countries around the world, thereby discouraging its usage. As a potential alternative to SF_6 , the compatibility of $C_5F_{10}O$ with conductive copper materials used in electrical equipment is of great significance in ensuring the safe and stable operation of environmentally friendly gas-insulated equipment. In this paper, the interaction among $C_5F_{10}O/N_2$, $C_5F_{10}O/air$ gas mixture, and copper was studied via experiments and simulations. When the $C_5F_{10}O/N_2$ (or air) gas mixture comes in contact with copper at the gas–solid interface, a small portion of $C_5F_{10}O$ is decomposed to form C_3F_6 (or C_3F_6 and C_3F_6O) at high temperatures. Meanwhile, at low temperatures ($120\text{ }^\circ\text{C}$), the $C_5F_{10}O/air$ gas mixture becomes more compatible with copper than with the $C_5F_{10}O/N_2$ gas mixture. When the experiment temperatures range between $170\text{ }^\circ\text{C}$ and $220\text{ }^\circ\text{C}$, the compatibility of the $C_5F_{10}O/air$ gas mixture with copper is significantly inferior to its compatibility with copper. Under high temperatures, the $C_5F_{10}O/air$ gas mixture shows severe corrosion on the copper surface due to the presence of O_2 , forms a thick cubic grain, and emits irritating gases. The simulations show that the carbonyl group in $C_5F_{10}O$ is chemically active and can be easily adsorbed on the copper surface. An anti-corrosion treatment must be performed on copper materials in manufacturing equipment. The findings provide an important reference for the application of $C_5F_{10}O$ gas mixture.

Keywords: $C_5F_{10}O$ gas mixture; SF_6 alternative gas; copper; compatibility; Cu_{13} nanocluster



Citation: Li, Y.; Zhang, X.; Xia, Y.; Li, Y.; Wei, Z.; Wang, Y.; Xiao, S. Study on the Compatibility of Eco-Friendly Insulating Gas $C_5F_{10}O/N_2$ and $C_5F_{10}O/Air$ with Copper Materials in Gas-Insulated Switchgears. *Appl. Sci.* **2021**, *11*, 197. <https://dx.doi.org/10.3390/app11010197>

Received: 22 November 2020

Accepted: 20 December 2020

Published: 28 December 2020

Publisher's Note: MDPI stays neutral with regard to jurisdictional claims in published maps and institutional affiliations.



Copyright: © 2020 by the authors. Licensee MDPI, Basel, Switzerland. This article is an open access article distributed under the terms and conditions of the Creative Commons Attribution (CC BY) license (<https://creativecommons.org/licenses/by/4.0/>).

1. Introduction

Since its application in medium- and high-voltage gas-insulated switchgears (GIS) in the 1930s [1], sulfur hexafluoride (SF_6) has been favored by the power industry for its excellent insulation and arc extinguishing performance. SF_6 is a gas-insulating medium that is frequently used in high-voltage electrical equipment, such as GIS and gas insulated lines [2]. However, the global warming potential (GWP) of SF_6 is 23,500 times higher than that of CO_2 . Given that SF_6 is chemically stable and difficult to decompose, its lifetime in the atmosphere can be as long as 3200 years [3,4]. As early as 1997, the “Kyoto Protocol” named SF_6 as one of the six greenhouse gases where usage needs to be restricted [5,6]. In addition, the Paris Agreement signed in 2016 requires the global average temperature to be controlled within two degrees Celsius above the pre-industrial temperature level.

The EU and other legislatures also listed SF₆ as a phase-out target [7]. The increasingly severe environmental situation has prompted researchers in the power industry to accelerate their search for environmentally friendly alternatives to SF₆ [8].

Replacing SF₆ with the perfluoroketone gas C₅F₁₀O and its gas mixture has attracted the attention of many scholars at home and abroad in recent years [9]. The insulation strength of C₅F₁₀O is twice that of SF₆, its GWP 100 value is less than one, its ozone depletion potential is zero, and its lifetime in the atmosphere is only 15 days. However, C₅F₁₀O has a higher liquefaction temperature (26.9 °C at normal pressure) compared with SF₆, thereby necessitating the mixture of this material with a buffer gas (N₂, air, and CO₂) with a low liquefaction temperature [10].

Many studies at home and abroad have examined C₅F₁₀O and its gas mixture. For instance, ABBTM tested the insulation properties of the C₅F₁₀O/air mixture and showed that the insulation performance of pure C₅F₁₀O is about twice that of SF₆. The C₅F₁₀O (39 kPa)/air mixture with a gas pressure of 0.7 MPa has an insulation strength of approximately 95% of that of SF₆ with a gas pressure of 0.45 MPa [11]. ABBTM also tested the insulation and breaking properties of the C₅F₁₀O/CO₂/O₂ mixture and found that the insulation performance of the C₅F₁₀O/CO₂/O₂ gas mixture is slightly lower than that of SF₆ and that its arc breaking performance is about 30% lower than that of SF₆. However, by increasing the total pressure of the C₅F₁₀O gas mixture, the electrical insulation strength can reach the equivalent insulation level of SF₆ [12]. Xiaohua Wang and Mingzhe Rong of Xi'an Jiaotong University tested the power frequency withstand voltage and lightning impulse performance of C₅F₁₀O/CO₂ and found that increasing the C₅F₁₀O content can effectively improve the insulation strength of the gas mixture and that increasing the total gas pressure of the C₅F₁₀O/CO₂ gas mixture can increase the lightning impulse discharge voltage [13]. Xingwen Li et al. calculated the thermodynamic properties and transmission coefficients of C₅F₁₀O/CO₂ mixtures and found that as the concentration of C₅F₁₀O increases, most thermophysical properties, including thermal conductivity, viscosity, and electrical conductivity, of C₅F₁₀O/CO₂ mixtures become closer to those of SF₆ [14]. Li Yi et al. calculated the stability and possible decomposition path of C₅F₁₀O molecules via a density functional theory simulation and detected decomposition products, such as CF₄, C₂F₆, C₃F₈, C₃F₆, C₄F₁₀, C₅F₁₂, and C₆F₁₄, by performing discharge experiments [15]. Xiao Dengming et al. calculated the plasma behavior of C₅F₁₀O/N₂ gas mixture under the assumption of local thermodynamic equilibrium. It is found that when the temperature is less than 7500 K, as the concentration of C₅F₁₀O increases, the enthalpy of gas mixture increases, and when the temperature exceeds 7500 K, the result is the opposite [16].

Although studies have investigated the insulation properties and arc extinguishing characteristics of the C₅F₁₀O gas mixture, only few have examined the compatibility of this gas mixture with metal materials. The insulating medium used in electrical equipment should show good compatibility with the metal materials inside this equipment. Copper is widely used as a conductive material in various equipment, including GIS. When using this equipment, the temperature of the conductive copper material increases due to the thermal effect of the current, whereas the poor contact of the conductive contacts may cause partial overheating [17,18]. Therefore, the compatibility of the C₅F₁₀O gas mixture with metal materials at different temperatures is of great significance in extending the service life and ensuring the safe and stable operation of equipment.

In this paper, a gas–solid compatibility experiment platform was designed to investigate the compatibility of C₅F₁₀O/N₂, C₅F₁₀O/air gas mixture, and copper materials when aging at different temperatures [19]. The surface morphology and element content of the gas decomposition products and copper samples after the experiments were studied by using a gas chromatography mass spectrometer (GC–MS), field emission scanning electron microscope (FESEM), and X-ray photoelectron spectroscopy (XPS). The interaction principle of the C₅F₁₀O on the Cu₁₃ nanocluster surface was calculated via simulation. The related findings provide a reference for the engineering application of C₅F₁₀O gas mixture instead of SF₆.

2. Experiment Platform

The experiment platform shown in Figure 1 mainly comprises a heating system, a temperature feedback monitoring control system, and a detection system. The heating system includes a heat source and a copper outer casing outside of the heat source, whereas the heat source transfers heat to the surface of the heating device through the copper outer casing. The copper shell has the same material as the experiment copper sheet sample, whereas the air chamber shell is made from stainless steel. To prevent the heating device from transmitting the high temperature to the inner wall of the air chamber, the heating device does not directly contact the air chamber wall, thereby avoiding stainless steel interference during the experiments. The temperature feedback monitoring control system includes a temperature sensor and a proportional–integral–derivative (PID) controller. The copper sample and temperature sensor for the PID controller feedback control are fixed on the copper casing to monitor the temperature of the copper sample in real time and to control the experiment process. The detection system includes GC–MS and FESEM. GC–MS is a GCMS-QP2010 Ultra manufactured by Shimadzu for analyzing the composition of matter in gas mixture. The column type, film thickness, length, inner diameter, inlet temperature, and mass ion source temperature were CP-SIL 5 CB, 8 μm , 60 m, 0.32 mm, 200 $^{\circ}\text{C}$, and 200 $^{\circ}\text{C}$, respectively [20]. This tool can also be used to check whether $\text{C}_5\text{F}_{10}\text{O}$ decomposes after coming in contact with the $\text{C}_5\text{F}_{10}\text{O}/\text{N}_2$ and $\text{C}_5\text{F}_{10}\text{O}/\text{air}$ gas mixture under different temperature conditions. FESEM is a Zeiss SIGMA FESEM produced by Carl Zeiss for observing the surface morphology of the test sample. The acceleration voltage range of FESEM is 0.1–30 kV, and the maximum resolution is 1.3 nm at 20 kV. The changes in the microstructure of the copper surface after coming into contact with the $\text{C}_5\text{F}_{10}\text{O}/\text{N}_2$ and $\text{C}_5\text{F}_{10}\text{O}/\text{air}$ gas mixture under different temperature conditions are also studied.

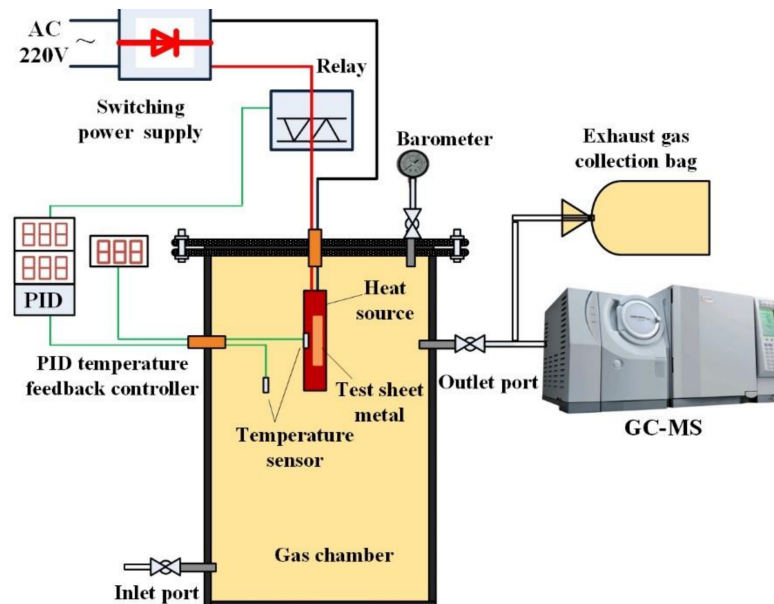


Figure 1. Experiment platform.

The copper samples were fastened to the surface of the copper casing before performing the experiments in order for the samples to adhere to the heat source during the experiments. The $\text{C}_5\text{F}_{10}\text{O}$ gas has a volume fraction of 7.5%. After the gas filling, the mixtures were allowed to stand for 24 h to thoroughly mix the gas mixture. The experiment group temperatures were 120 $^{\circ}\text{C}$, 170 $^{\circ}\text{C}$, and 220 $^{\circ}\text{C}$, whereas the heating time was 8 h. After 1 h of natural cooling, the experiment was terminated. Given that the $\text{C}_5\text{F}_{10}\text{O}$ gas at a pressure of 0.1 MPa had a liquefaction temperature of 26.9 $^{\circ}\text{C}$, the compatibility of the pure $\text{C}_5\text{F}_{10}\text{O}$ gas with the copper material at a gas pressure of 0.3 MPa cannot be studied.

Therefore, the pressure of the pure $C_5F_{10}O$ gas was set to 0.1 MPa for the experimental group, and the results are compared with those of the $C_5F_{10}O/N_2$ and $C_5F_{10}O$ /air gas mixture experimental group.

3. Experiment

A photo of the copper samples after the $C_5F_{10}O/N_2$ gas mixtures came in contact with the copper material under high temperature conditions is presented in Figure 2. The copper material in the control group before the experiment was purple-red and bright in color. When the experiment temperatures range between 120 °C and 170 °C, the copper surface color gradually turns golden yellow. When the experiment temperature is 220 °C, the copper surface color turns pink.

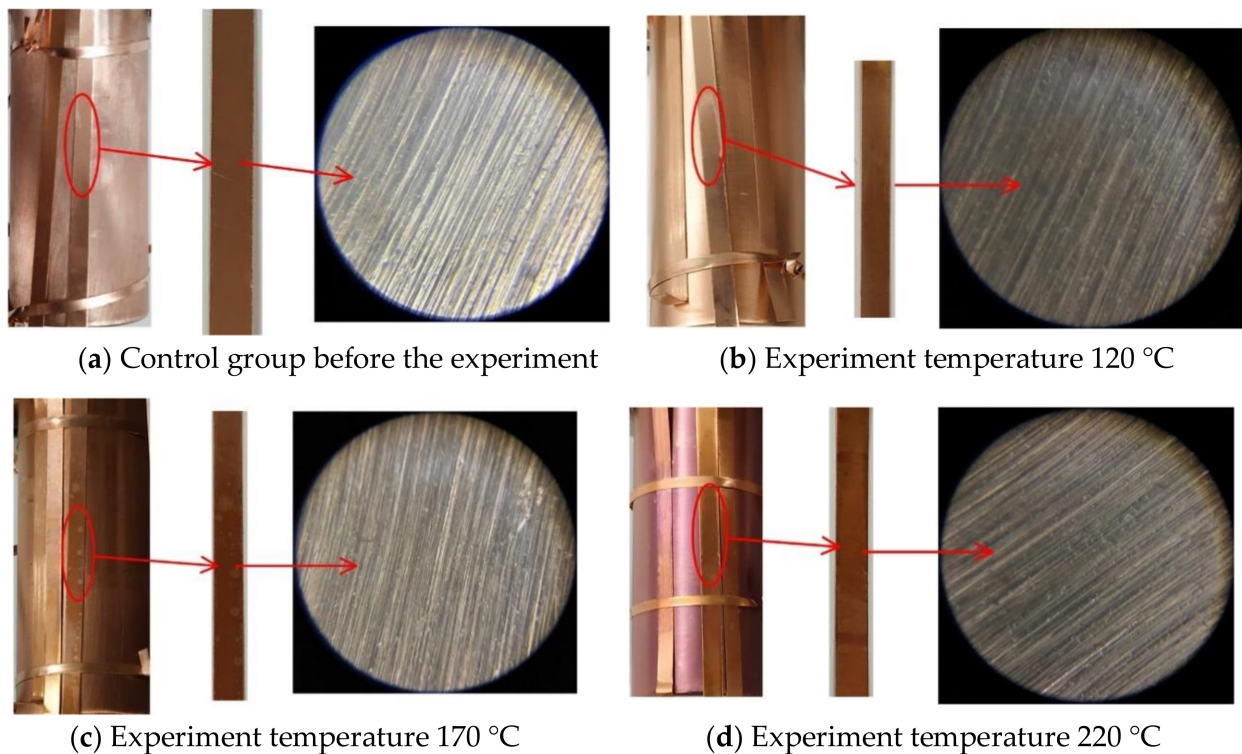


Figure 2. Surface photo of copper before and after contact with $C_5F_{10}O/N_2$ gas mixture.

Figure 3 shows the change in the color of the copper surface after the $C_5F_{10}O$ /Air gas mixture comes in contact with the copper sample under different experiment temperature conditions. Meanwhile, Figure 3a shows that the copper surface of the pure $C_5F_{10}O$ experimental group is brown and uniform in color. One can observe through optical microscopy that the copper surface is darkened and that the metallic luster is lost. The original fine lines on the surface of the copper sample are covered by the corrosion layer, and the corrosion layer is thicker than the other experiment groups. Therefore, the pure $C_5F_{10}O$ gas has poor compatibility with copper. Figures 2d and 3e show that the $C_5F_{10}O$ /air gas mixture at an experiment temperature of 120 °C has a similar color to the copper surface of the $C_5F_{10}O/N_2$ gas mixture experiment group at an experiment temperature of 220 °C. When the experiment temperature is 170 °C, the copper casing of the heat source turns red, whereas the copper sheet fixed on the surface turns brown. When the experiment temperature is 220 °C, the surface color of the copper turns dark brown and a strong pungent odor is emitted. The change in the color of the copper surface is most obvious at this time.

The color of the copper surface turned red or pink in the experiment mainly because the copper on the surface was oxidized to red cuprous oxide. As the temperature increased, the cuprous oxide further oxidized to black copper oxide. Meanwhile, the change in the

color of the copper surface from purple to red or from pink to black in the experiment was due to the continuous oxidation of copper.

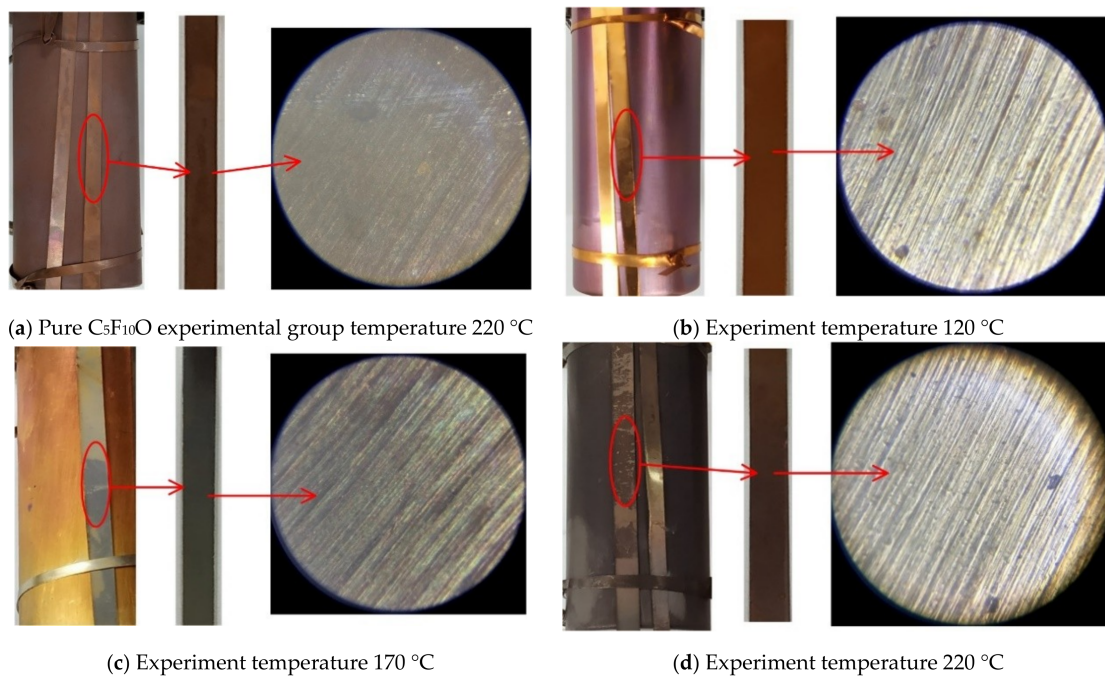


Figure 3. Surface photo of copper before and after contact with C₅F₁₀O/air gas mixture.

4. Results Characterization

4.1. GC–MS Results

In the presence of metallic copper, certain chemical reactions may lead to the decomposition of C₅F₁₀O, and these reaction products can be analyzed by GC–MS. After the end of the experiments, the sample gas bag was used to collect the gas sample inside the reaction vessel for the gas chromatography mass spectrometry, and the obtained chromatogram is shown in Figure 4. Given that the decomposition products of the C₅F₁₀O gas mixture have unknown compositions after they come in contact with copper under superheated conditions, all possible decomposition products were scanned by using SCAN mode during the GC–MS analysis and were tested for qualitative analysis. To avoid the interference of N₂, H₂O, and CO₂ in the air, the small molecular substances with a mass-to-charge ratios (*m/z*) of less than 44 were not considered in the mass spectrometry.

As shown in Figure 4a and Table 1, the C₅F₁₀O/N₂ gas mixture of the experiment group was partially decomposed when it came into contact with the copper surface at a high temperature. The mass spectrum corresponding to the peak of 5.762 min to 5.964 min obtained an *m/z* = 131, the molecular ion obtained *m/z* = 150, and the matching molecule was searched for C₃F₆ by using the National Institute of Science and Technology (NIST) standard reference database 14.0. The mass spectrum corresponding to the peak of 6.013 min to 6.373 min obtained *m/z* = 69, and the matching molecule was searched for C₃F₇H.

Figure 4b shows that the C₅F₁₀O/air gas mixture comes in contact with the copper surface at a high temperature, the decomposition of C₅F₁₀O is similar to that shown in Figure 4a, and that C₃F₆ is detected. The difference is that the C₅F₁₀O/air gas mixture experiment group produced C₃F₆O and C₃F₇H. The GCMS results show that the C₅F₁₀O reacted at the gas–solid interface at high temperature to break the chemical bond of C₅F₁₀O, to form small fragment particles, and to produce a series of decomposition products. The pure C₅F₁₀O not only detected the above decomposition products but also separated CF₄ at 5.106 min to 5.295 min, and no CF₄ was detected in the C₅F₁₀O/N₂ and C₅F₁₀O/air

gas mixture experimental group. Both N_2 and air act as buffer gases that affect the decomposition reaction of $C_5F_{10}O$ at high temperatures and inhibit the production of CF_4 . At the same time, with the presence of O_2 in N_2 and air, the gas mixture also showed different chemical properties.

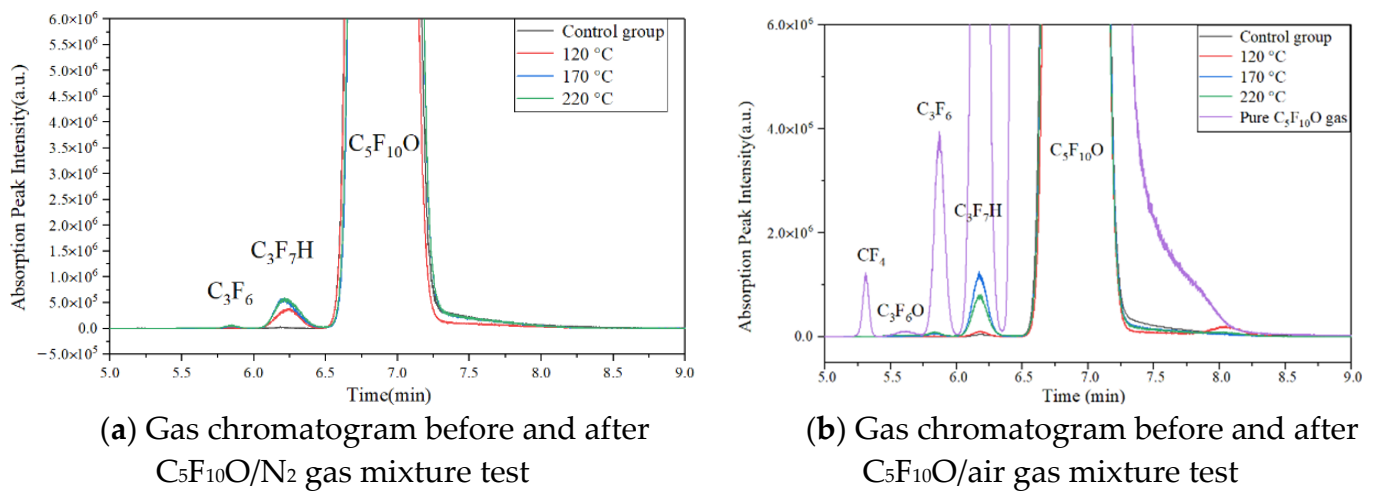


Figure 4. Gas chromatogram of $C_5F_{10}O$ gas.

Table 1. $C_5F_{10}O$ gas and its decomposition product mass-to-charge ratios (m/z) and separation time.

Gas Type	Mass-to-Charge Ratios (m/z)	Separation Time (min)
$C_5F_{10}O$	69, 97, 169, 197, 266	6.423–7.254
C_3F_7H	69, 151	6.013–6.373
C_3F_6	69, 100, 131, 150	5.762–5.964
CF_4	51, 69	5.106–5.295
C_3F_6O	69, 97, 147	5.339–5.631

4.2. FESEM Characterization

At the end of the experiment, the copper samples were taken out and their surface topography was characterized by FESEM. The surface photomicrographs are shown in Figures 5 and 6.

Figure 5 shows the surface morphology of copper in the $C_5F_{10}O/N_2$ gas mixture experiment group and the control group. In the control group, the copper surface is smooth and flat, while its structure is fine and compact. The small grooves appearing under the microstructure are inevitable due to the limitations of the manufacturing process. When the experiment temperature is 120 °C, corrosion spots appear on some parts of the copper surface. Figure 5b presents the morphology of the corrosion point, which in turn shows an island-like irregular distribution in the field of view and a flat crystal structure. When the experiment temperature is 170 °C, the distribution of the corrosion points gradually increases while its distribution remains relatively uniform. The crystal structure of the corrosion points in the entire field of view becomes more three-dimensional, and the crystal exhibits a certain regularity. When the experiment temperature is 220 °C, the corrosion layer evenly covers the entire copper surface, and the density of the corrosion point increases. However, the corrosion layer remains in the shallow region of the copper surface during the experiment.

When the copper surface temperature increases, the corrosion point is initially concentrated in the position where the copper surface has a small flaw. As the temperature increases, the corrosion point gradually spreads across the surface of the copper sample. The temperature further increases, and the corrosion point becomes dense, thereby covering the entire copper surface.

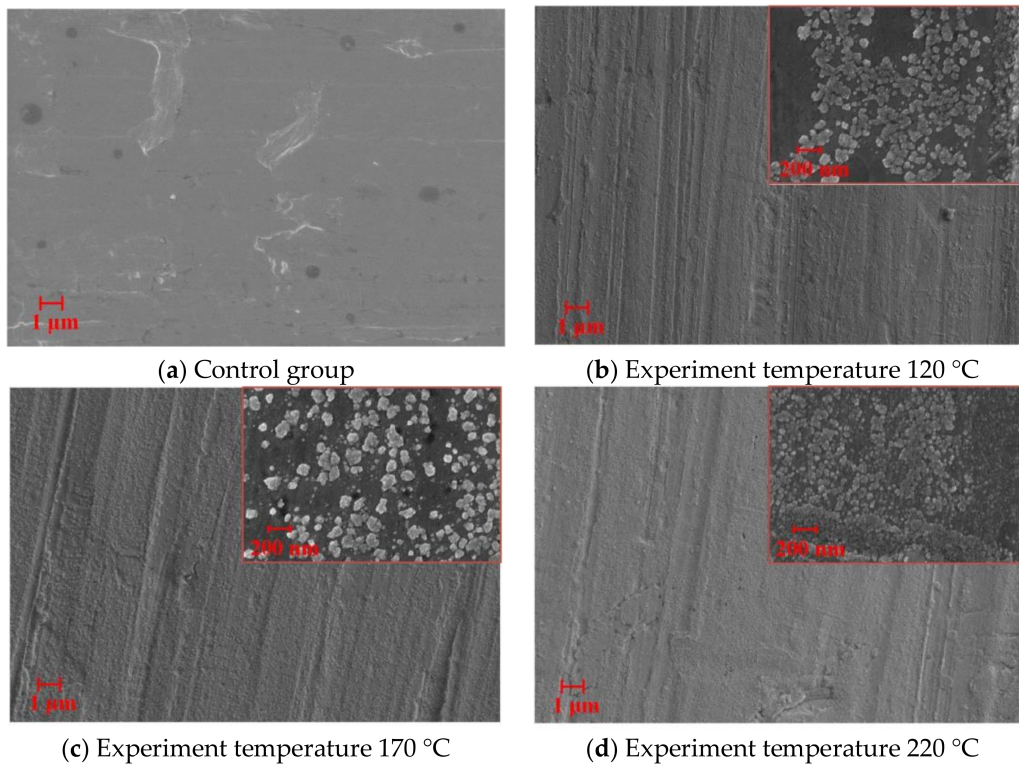


Figure 5. FESEM morphology of the surface after contact of copper with $C_5F_{10}O/N_2$ gas mixture.

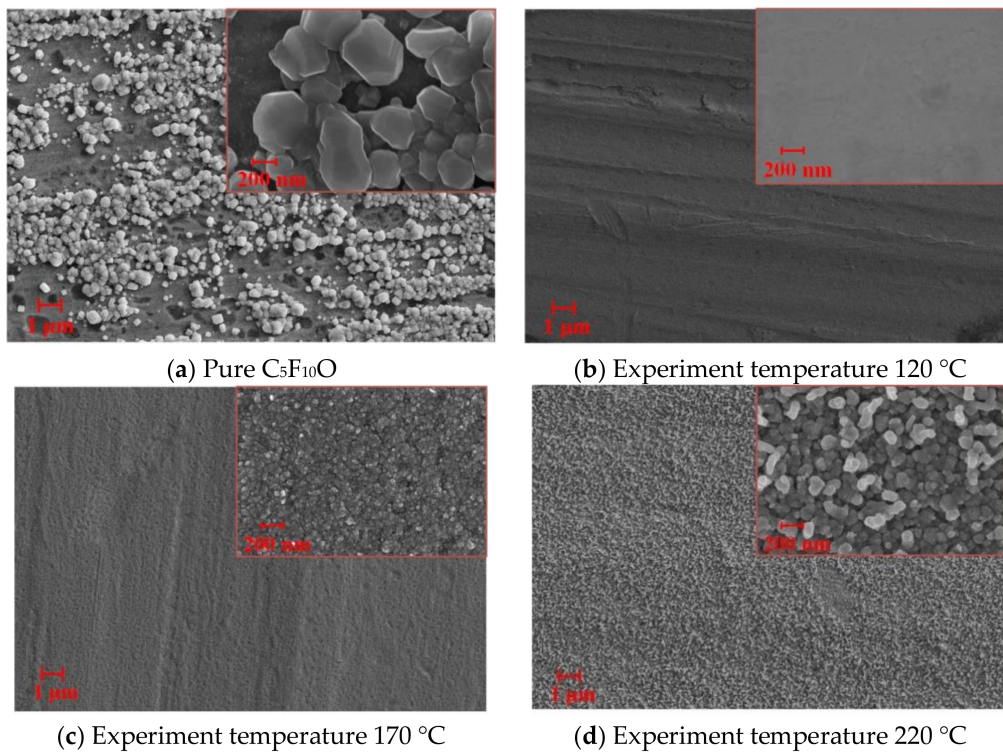


Figure 6. FESEM morphology of the surface after contact of copper with $C_5F_{10}O/air$ gas mixtures.

Figure 6 shows the surface morphology of the copper in the $C_5F_{10}O/air$ gas mixture experiment group and the pure $C_5F_{10}O$ experiment group. When viewed under an electron microscope, the surface of the copper sample of the pure $C_5F_{10}O$ experimental group is

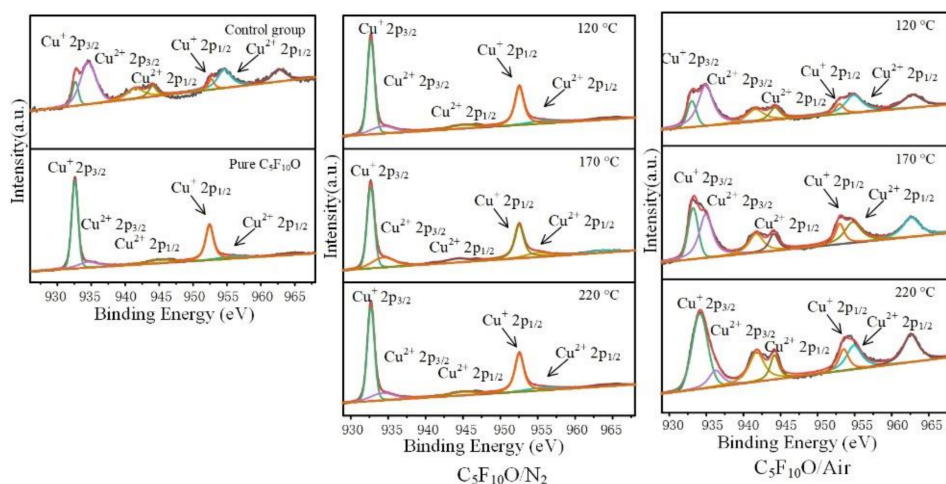
very corroded, and at high magnification, coarse and irregular cubic grains are observed on the surface. When the experiment temperature of the $C_5F_{10}O$ /air gas mixture experiment group is $120\text{ }^\circ\text{C}$, no obvious corrosion point is observed on the copper surface. The copper surface color of the $C_5F_{10}O$ /air gas mixture experiment group at $120\text{ }^\circ\text{C}$ becomes similar to that of the $C_5F_{10}O/N_2$ gas mixture experiment group at a temperature of $220\text{ }^\circ\text{C}$. However, the micrograph does not show a similar morphology, thereby suggesting that the change in the color of the copper surface cannot accurately determine whether the copper is corroded. Therefore, FESEM testing must be applied on the copper samples. When the experiment temperature is $170\text{ }^\circ\text{C}$, a dense cubic block crystal appears on the copper surface, thereby suggesting a severe corrosion on the copper surface. Meanwhile, when the experiment temperature is $220\text{ }^\circ\text{C}$, a rough and uniform crystal is observed on the surface when viewed under a microscope, and a more serious degree of corrosion is recorded.

The differences in the compatibility of the $C_5F_{10}O/N_2$ gas mixture and the $C_5F_{10}O$ /air gas mixture with copper can be mainly attributed to the action of O_2 . Researchers from ABBTM have proposed that in accordance with the requirements of International Electrotechnical Commission (IEC) 62271-200, O_2 , as part of the insulating medium in the $C_5F_{10}O$ /air mixture, must be silver-plated at the contacts through which the primary current flows in the electrical equipment [21]. As a buffer gas, N_2 has high stability and low liquefaction temperature. This gas is chemically inert and does not participate in the chemical reaction between $C_5F_{10}O$ and copper. Therefore, the surface morphology of the $C_5F_{10}O/N_2$ gas mixture after coming in contact with copper at different experiment temperatures can be mainly ascribed to the reaction of $C_5F_{10}O$ with metallic copper at high temperatures. Due to the presence of O_2 in the air, the $C_5F_{10}O$ /air gas mixture experiment group shows a high chemical stability at $120\text{ }^\circ\text{C}$ and exhibits good compatibility at low temperatures. However, at high temperatures, copper reacts with O_2 to form metal oxide.

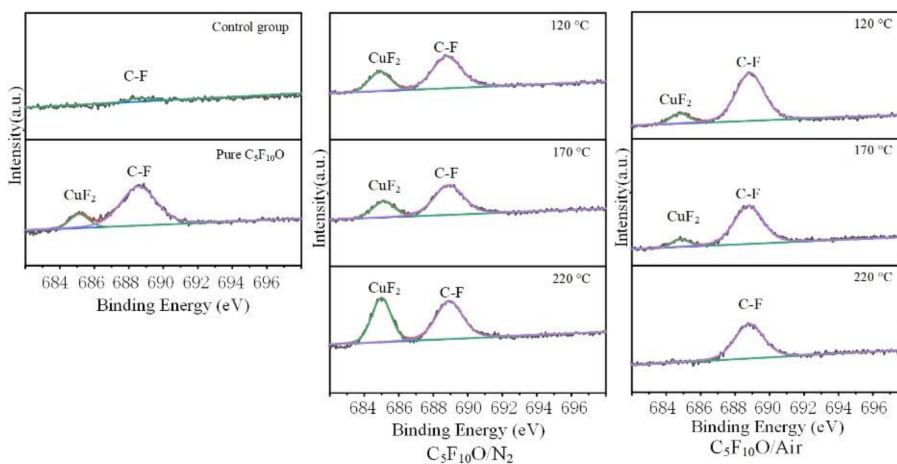
4.3. XPS Characterization

To further study the changes in the elements (Cu 2p, F 1s, C 1s, O 1s, and N 1s) and materials on the surface of copper samples, an energy spectrum scanning test was performed with XPS. The best spatial resolution of XPS is better than $20\text{ }\mu\text{m}$, and the imaging spatial resolution is better than $3\text{ }\mu\text{m}$. The track of the element being tested was selected according to internationally accepted test rules. After using the XPS Peak software to perform a Shirley-type fitting deduction on the energy spectrum background [22], the Gaussian algorithm was used for peak fitting, and the chemical state of the element was determined by using the National Institute of Standards and Technology (NIST) XPS database and previous studies as references [23–25].

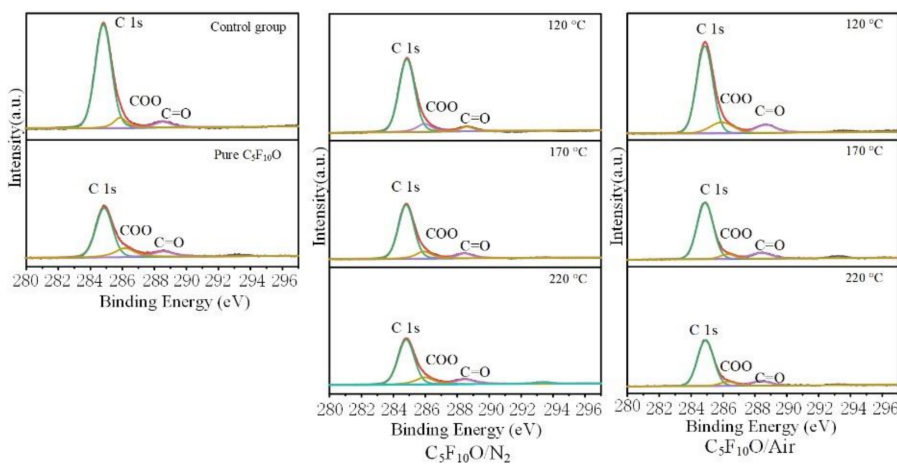
Figure 7a presents the photoelectron spectroscopy curve of the 2p orbital of Cu element on the surface of a copper sample. After the peak photo-matching of the secondary photoelectron emission peak of the copper element, the five peaks with electron binding energies of 932.7, 934.6, 944.8, 952.5, and 952.7 eV were $Cu_2O\ 2p_{3/2}$, $CuO\ 2p_{3/2}$, $CuO\ 2p_{3/2}$, $Cu_2O\ 2p_{1/2}$, and $CuO\ 2p_{1/2}$, respectively. The secondary photoelectron emission peak at 954.90 eV in Figure 7a exceeds the photoelectron binding energy generated by the transition of the Cu element level. Therefore, this peak should be the photoelectron emission peak of the other elements. The change in CuO and Cu_2O content in Figure 7a corresponds to the change in the color of the copper surface. The copper energy spectrum scanning results indicate that the surface of the copper sample mainly contains CuO and Cu_2O produced via oxidation of the copper surface. Copper and pure $C_5F_{10}O$ and $C_5F_{10}O/N_2$ gas mixtures react at high temperatures to form CuF_2 (Figure 7b). Some Cu also reacts with the $C_5F_{10}O/N_2$ gas to form compounds that contain Cu, C, and N (Figure 7e). The surface copper detection results recorded at $120\text{ }^\circ\text{C}$ are consistent with the control group, thereby indicating that copper shows good compatibility with the $C_5F_{10}O$ /air gas mixture at $120\text{ }^\circ\text{C}$ (the XPS test results are consistent with the FESEM results). Some Cu participates in the reaction as the experimental temperature increases.



(a) Cu 2p

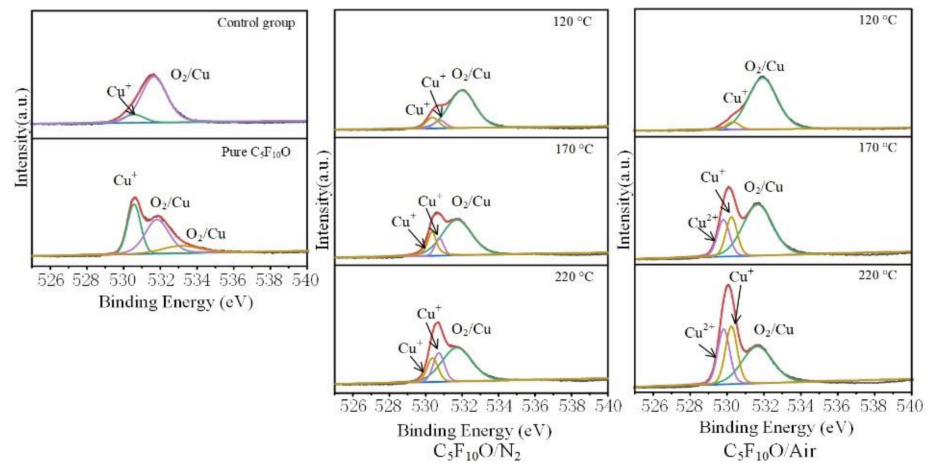


(b) F 1s

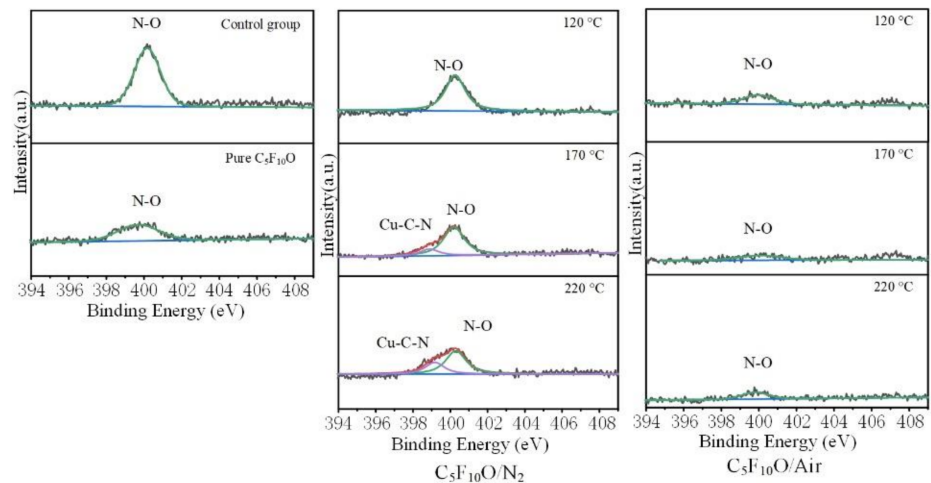


(c) C 1s

Figure 7. Cont.



(d) O 1s



(e) N 1s

Figure 7. Copper surface element XPS energy spectrum.

Figure 7b presents the photoelectron spectroscopy of the 1s orbital of the F element on the surface of the copper sample. No F element was detected in the control group. In the pure $C_5F_{10}O$ experimental group, some $C_5F_{10}O$ was decomposed on the copper surface at a high temperature, and CuF_2 and C–F bonds were detected at binding energies of 684.7 eV and 688.8 eV. The detected CuF_2 is a product of the reaction of $C_5F_{10}O$ molecules with CuO on the copper surface. CuF_2 and C–F bonds were detected in the $C_5F_{10}O/N_2$ experiment group, thereby suggesting that the $C_5F_{10}O/N_2$ gas mixture reacted with copper at an elevated temperature and that the relative content of CuF_2 and C–F bonds increased along with the experiment temperature. By contrast, the $C_5F_{10}O/air$ gas mixture experiment group tended to decrease the relative content of CuF_2 and C–F bonds as the experiment temperature increased. CuF_2 was not detected at 220 °C, and the fluorine element on the copper surface was mainly present as a C–F bond. In the experiment group, the fluorine element mainly existed in the form of a C–F bond, a small amount of fluorine existed in the form of CuF_2 , and the C–F bond did not show much difference across each experimental group. The C–F bond may be a $C_5F_{10}O$ molecule adsorbed on the surface of a copper sample or a small molecule product containing C and F that was produced after the decomposition of $C_5F_{10}O$.

Figure 7c presents the photoelectron spectroscopy of the 1s orbital of the C element on the surface of the copper sample. The energy peaks detected at photoelectron binding energies of 284.70, 286.30, and 286.60 eV were C 1s, COO, and C=O, respectively. The peaks of COO and C=O did not differ between the control group and each experimental group, and the relative content of the C 1s peak was slightly reduced.

Figure 7d presents the photoelectron spectroscopy of the 1s orbital of the O element on the surface of the copper sample. In the C₅F₁₀O/air gas mixture experiment groups, the three peaks with electron binding energies of 529.8, 530.3, and 531.8 eV were Cu²⁺(CuO or CuF₂), Cu⁺(Cu₂O), and O₂/Cu (oxygen on copper, O₂⁻, O²⁻ or O⁻), respectively. In other gas mixture experiment groups or the control group, Cu⁺(Cu₂O) was detected at photoelectron binding energies of 530.3 eV and 530.7 eV. O₂/Cu (oxygen on copper, O₂⁻, O²⁻ or O⁻) was detected at photoelectron binding energies of 531.8 eV and 532.9 eV. Cu²⁺ (or Cu⁺) with different binding energies are copper oxide or cuprous oxide crystals of different crystal types, and the oxygen on copper was detected in the control group because oxygen in the air was adsorbed on the surface.

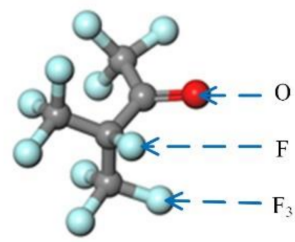
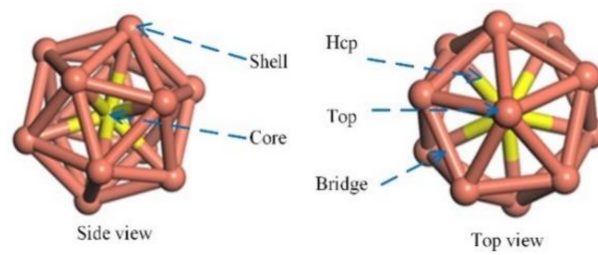
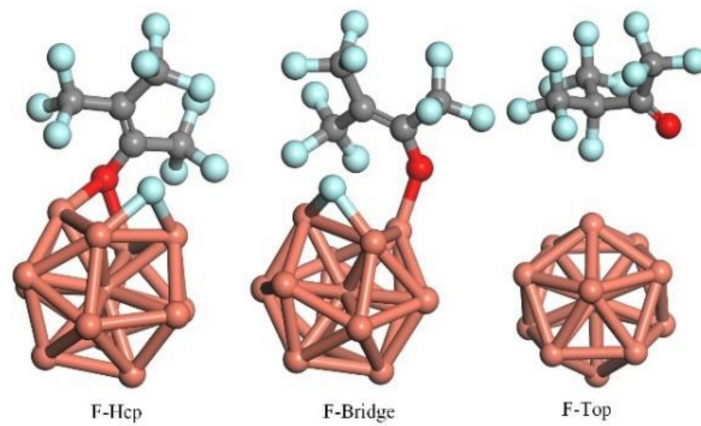
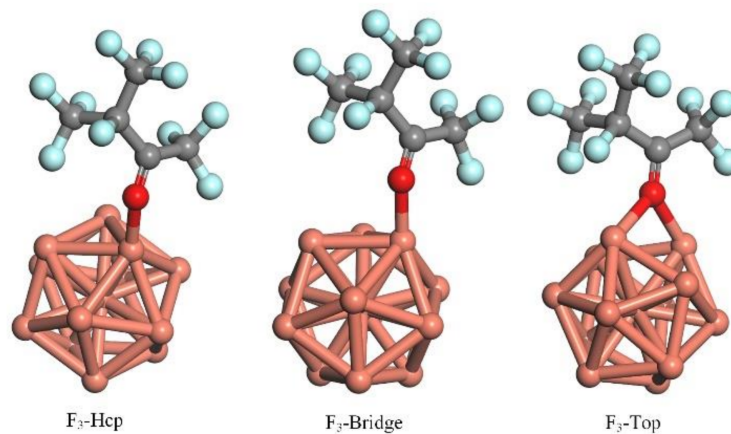
Figure 7e presents the photoelectron spectroscopy of the N-element 1s orbital of the copper sample surface. Cu–C–N compounds and N–O bonds were detected at photoelectron binding energies of 398.60 eV and 400.10 eV. As the experiment temperature increased, the relative content of the N–O bond gradually decreased and an N–O bond was not detected in the C₅F₁₀O/air gas mixture experiment group at high temperatures. Meanwhile, a Cu–C–N compound was detected in the C₅F₁₀O/N₂ gas mixture experiment group.

The results of the XPS test reveal that C₅F₁₀O reacts with Cu at the gas–solid interface and that C₅F₁₀O reacts differently with N₂ and air buffer gas. This finding is consistent with the results of previous research.

5. Simulations

C₅F₁₀O and Cu reacted at the gas–solid interface. To further understand the interaction mechanism between C₅F₁₀O and Cu, a theoretical calculation was performed based on density functional theory (DFT) by using the DMol³ module of Materials Studio [26,27]. The Dmol³ module is a unique DFT quantum mechanics software that can study gas phase, solution, surface, and solid systems. Furthermore, the Dmol³ module is the fastest in molecular density functional calculation, which can quickly optimize the structure of molecules and solid systems, saving calculation time and other advantages. Copper clusters have many isomers, and the number of isomers rapidly increases along with the number of atoms in the cluster. Cu₁₃ clusters were selected for the calculation. According to previous studies [28–30], the icosahedron structure that comprises 13 copper atoms is considered the most stable (Figure 8a). In this structure, 12 copper atoms form an icosahedral shell and the most stable Cu₁₃ nanoclusters with a core copper atom. The copper atoms on the outer shell have a coordination number of six. Therefore, the Cu₁₃ nanocluster only has three adsorption sites, namely top, bridge, and Hcp (Figure 8b). Generalized gradient approximation with the Perdew–Burke–Ernzerhof function was employed to calculate the electronic exchange correlation, and the double numerical plus basis set with a polarization d-function was used to expand the valence electron functions. The smearing value was set as 0.005 Ha. To determine the accurate activation barrier of the Cu and C₅F₁₀O reaction, the complete linear synchronous transit and quadratic synchronous transit (LST/QST) approach was used to search for the transition state of the Cu and C₅F₁₀O reaction [31,32].

The molecular structure of C₅F₁₀O suggests that C₅F₁₀O has three adsorption sites, namely O, F, and F₃ (Figure 8a). Therefore, the C₅F₁₀O and Cu₁₃ nanoclusters have nine adsorption modes, and the calculation results are shown in Figure 8c–e.

(a) $C_5F_{10}O$ (b) Cu_{13} nanocluster(c) $F-Cu_{13}$ nanocluster(d) F_3-Cu_{13} nanocluster

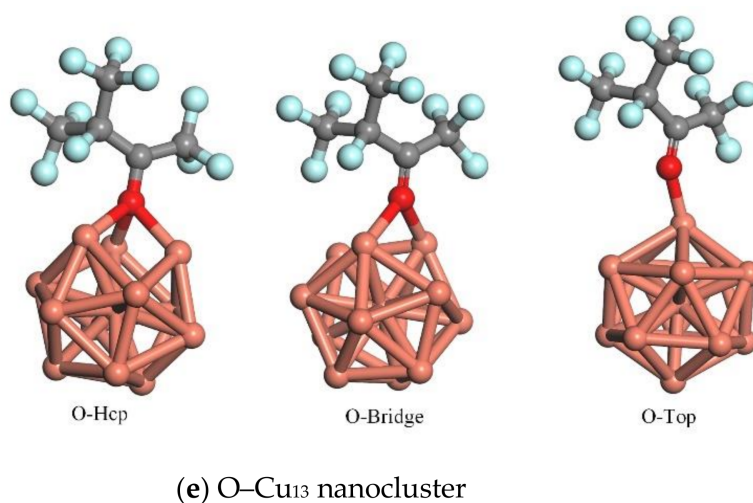


Figure 8. Simulation results of the reaction process between C₅F₁₀O and copper.

Before the calculation, the target atom in C₅F₁₀O was given a distance from the Cu₁₃ nanocluster core-shell structure, and then the intermolecular adsorption was calculated. Figure 8c shows that the F in Figure 8a can react with the Cu₁₃ nanocluster at the bridge and Hcp adsorption sites of the Cu₁₃ nanocluster to form a chemical bond with the Cu nanocluster, thereby resulting in the cleavage of the C–F bond of the alpha (α) carbon atom. At the same time, given the close position of the upper F and O atoms in the C₅F₁₀O molecular space structure, when the distance between the F atom and the Cu₁₃ nanocluster is small, the distance between the O atom and Cu₁₃ nanocluster is also small. The chemical nature of the carbonyl group is relatively active. In the chemical reaction, the C=O double bond is easily broken. Therefore, O reacts with the Cu nanocluster to break the C=O double bond and to form a Cu–O metal ion bond. The carbon of the carbonyl group combines with the carbon atom at the alpha position to form a carbon–carbon double bond (Figure 8e). At the top adsorption site, only one Cu atom in the Cu₁₃ nanocluster is located close to the C₅F₁₀O molecule, and F cannot form a chemical bond with the Cu nanocluster. The calculations reveal that only the carbonyl group reacts with Cu to break the carbon–oxygen double bond into a single bond and that the F atom on the α-position carbon atom can react with the Cu nanocluster to break the fluorocarbon bond at the α-position carbon atom and form a carbon–carbon double bond.

Figure 8d reveals that the chemical properties of CF₃–(trifluoromethyl) are relatively stable and cannot be adsorbed at the three adsorption sites of the Cu₁₃ nanocluster. When close to the Cu₁₃ nanocluster, the oxygen atom of the carbonyl group is adsorbed and interacted. This result also reflects the chemical activity of the oxygen atom on the carbonyl group of C₅F₁₀O. This conclusion is verified in Figure 8e. At the Hcp adsorption site, the carbon–oxygen double bond of the carbonyl group is broken, and O interacts with three copper atoms. The three Cu atoms demonstrate a strong attraction to electrons, thereby breaking the carbon–oxygen double bond and forming an ionic bond. Two and one Cu atoms interact with O at the bridge and top adsorption sites, respectively. When the number of Cu atoms is less than three, the attraction to the outer electrons of the O atom is insufficient to break the carbon–oxygen double bond of the carbonyl group. Therefore, the O atom forms a covalent bond with one or two copper atoms in the Cu₁₃ nanocluster.

The above calculation results and analysis reveal that C₅F₁₀O decomposes on the surface of the Cu₁₃ nanocluster. Figure 9 shows the total energy change of the system before and after the calculation. The statistical value is computed as the difference between the energies of the product and reactant. Figure 9 shows that energy is released during the above reaction, with the energy released at the F-bridge and F-Hcp adsorption sites being the highest, thereby suggesting that these two reactions are most likely to occur. The detection of C₃F₆ in the previous GC–MS results also demonstrates that the reaction at

the F-bridge and F-Hcp adsorption sites has resulted in the formation of a carbon–carbon double bond (C=C).

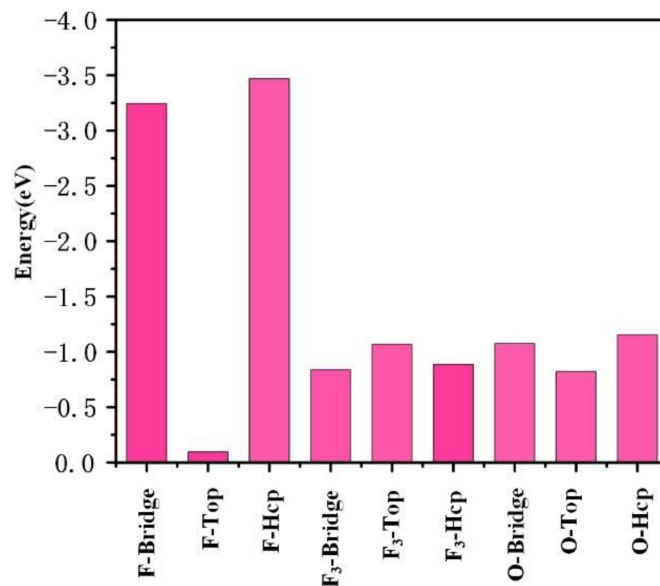


Figure 9. Total energy change before and after simulation calculation.

6. Conclusions

C₅F₁₀O/N₂ and C₅F₁₀O/air mixtures have good application prospects as electrical insulating mediums that can replace SF₆. Studying the compatibility of materials before their application in engineering practice is of great significance to ensure the safe and stable operation of electrical equipment throughout their design lifecycle. In this paper, the compatibility of the environmentally friendly insulating medium C₅F₁₀O/N₂, C₅F₁₀O/air gas mixture, and metallic material copper inside GIS equipment at different temperatures (120 °C to 220 °C) was examined. The test gas and copper samples were analyzed via GC–MS and FESEM characterization, and the interaction between the C₅F₁₀O and Cu₁₃ nanoclusters was calculated via a simulation. The following conclusions were drawn:

- (1) When the experiment temperature varies between 120 °C and 220 °C, the surface color of the copper material of the C₅F₁₀O/N₂ gas mixture experimental group changes from purple to golden yellow and then to pink. In the C₅F₁₀O/air gas mixture experimental group, the surface color of the copper material changes from purple to brown and then to dark brown as irritating gases are emitted.
- (2) The GC–MS characterization results show that the C₅F₁₀O/N₂ and C₅F₁₀O/air gas mixtures have a small amount of C₅F₁₀O decomposition. The C₅F₁₀O/N₂ gas mixture decomposes to produce C₃F₆ and C₃F₇H, and the C₅F₁₀O/air gas mixture decomposes to produce C₃F₆, C₃F₇H and C₃F₆O.
- (3) The FESEM characterization results show that the compatibility of the C₅F₁₀O/air gas mixture with copper at a low experiment temperature (120 °C) is better than that of the C₅F₁₀O/N₂ gas mixture with copper. However, due to the effect of O₂, when the experiment temperature is high (170 °C and 220 °C), the compatibility of the C₅F₁₀O/Air gas mixture with copper is significantly inferior when compared with that of C₅F₁₀O/N₂ gas mixture and copper. Therefore, when using the C₅F₁₀O/air gas mixture as the insulating medium in engineering applications, special attention should be paid to the condition of the copper material inside the equipment when local overheating occurs. At the same time, operation and maintenance personnel should wear gas masks to prevent the inhalation of toxic decomposition products from harming their health.

- (4) The molecular adsorption of the $C_5F_{10}O$ and Cu_{13} nanocluster is an exothermic reaction. The F atom on the α -position carbon atom of the $C_5F_{10}O$ molecule and the oxygen atom on the carbonyl group have high chemical activity and are most likely to interact with Cu during the interaction process.

Author Contributions: Conceptualization, X.Z. and Y.L. (Yalong Li); methodology, Y.L. (Yalong Li); software, Y.L. (Yalong Li); validation, Y.L. (Yalong Li), Z.W. and Y.W.; formal analysis, Y.L. (Yalong Li); investigation, Y.L. (Yalong Li); resources, Y.L. (Yalong Li); data curation, Y.L. (Yalong Li); writing—original draft preparation, Y.L. (Yalong Li); writing—review and editing, X.Z. and Y.L. (Yi Li); visualization, Y.X.; supervision, X. Z.; project administration, S.X. All authors have read and agreed to the published version of the manuscript.

Funding: This research was funded by Science and Technology Project of State Grid Sichuan Electric Power Company, grant number 4Z20W1970018.

Data Availability Statement: The data presented in this study are available in article.

Acknowledgments: Yalong Li thanks the support from the China Scholarship Council (grant no. 202006270108).

Conflicts of Interest: The authors declare no conflict of interest

References

- Zhang, G.; Zhang, X.; Cheng, H.; Tang, J. Ladder-Wise calculation method for z -coordinate of transformer PD source based on planar layout UHF antenna sensors. *IEEE Trans. Electr. Electron. Eng.* **2020**, *15*, 340–345. [[CrossRef](#)]
- Li, Y.; Zhang, Y.; Li, Y.; Tang, F.; Lv, Q.; Zhang, J.; Xiao, S.; Tang, J.; Zhang, X. Experimental study on compatibility of eco-friendly insulating medium $C_5F_{10}O/CO_2$ gas mixture with copper and aluminum. *IEEE Access* **2019**, *7*, 83994–84002. [[CrossRef](#)]
- Zhang, Y.; Li, Y.; Cui, Z.; Chen, D.; Zhang, X. Simulation and experiment on the catalytic degradation of high-concentration SF_6 on TiO_2 surface under UV light. *AIP Adv.* **2018**, *8*, 055215. [[CrossRef](#)]
- Andersen, M.P.S.; Kyte, M.; Andersen, S.T.; Nielsen, C.J.; Nielsen, O.J. Atmospheric chemistry of $(CF_3)_2CF-C\equiv N$: A replacement compound for the most potent industrial greenhouse gas, SF_6 . *Environ. Sci. Technol.* **2017**, *51*, 1321–1329. [[CrossRef](#)] [[PubMed](#)]
- Xiao, S.; Gao, B.; Pang, X.; Zhang, X.; Li, Y.; Tian, S.; Tang, J.; Luo, Y. The sensitivity of C_4F_7N to electric field and its influence to environment-friendly insulating gas mixture C_4F_7N/CO_2 . *J. Phys. D Appl. Phys.* **2021**, *54*, 055501. [[CrossRef](#)]
- Reilly, J.; Prinn, R.G.; Harnisch, J.; Fitzmaurice, J.; Jacoby, H.D.; Kicklighter, D.; Melillo, J.; Stone, P.H.; Sokolov, A.P.; Wang, C. Multi-gas assessment of the Kyoto Protocol. *Nature* **1999**, *401*, 549–555. [[CrossRef](#)]
- Mong, R. *Investigation of Electrical Properties of a New Low-GWP Insulation Gas-Comparison of AirPlus and Synthetic Air*; NTNU: Trondheim, Norway, 2018.
- Romero, A.; Racz, L.; Matrai, A.; Bokor, T.; Cselko, R. A review of sulfur-hexafluoride reduction by dielectric coatings and alternative gases. In Proceedings of the 2017 6th International Youth Conference on Energy (IYCE), Budapest, Hungary, 21–24 June 2017; pp. 1–5.
- Mantilla, J.; Claessens, M.; Kriegel, M. *Environmentally Friendly Perfluoroketones-Based Mixture as Switching Medium in High Voltage Circuit Breakers*; Paper A3-113; CIGRE: Paris, France, 2016.
- Li, Y.; Zhang, X.; Wang, Y.; Li, Y.; Zhang, Y.; Wei, Z.; Xiao, S. Experimental study on the effect of O_2 on the discharge decomposition products of $C_5F_{10}O/N_2$ mixtures. *J. Mater. Sci. Mater. Electron.* **2019**, *30*, 19353–19361. [[CrossRef](#)]
- Simka, P.; Ranjan, N. Dielectric strength of C_5 perfluoroketone. In Proceedings of the 19th International Symposium on High Voltage Engineering, Pilsen, Czech Republic, 23–28 August 2015; pp. 23–28.
- Stoller, P.C.; Doiron, C.B.; Tehlar, D.; Simka, P.; Ranjan, N. Mixtures of CO_2 and $C_5F_{10}O$ perfluoroketone for high voltage applications. *IEEE Trans. Dielectr. Electr. Insul.* **2017**, *24*, 2712–2721. [[CrossRef](#)]
- Zhong, J.; Fu, X.; Yang, A.; Han, G.; Liu, J.; Lu, Y.; Wang, X.; Rong, M. Insulation performance and liquefaction characteristic of $C_5F_{10}O/CO_2$ gas mixture. In Proceedings of the 2017 4th International Conference on Electric Power Equipment—Switching Technology (ICEPE-ST), Xi'an, China, 22–25 October 2017; pp. 291–294.
- Li, X.; Guo, X.; Murphy, A.B.; Zhao, H.; Wu, J.; Guo, Z. Calculation of thermodynamic properties and transport coefficients of $C_5F_{10}O-CO_2$ thermal plasmas. *J. Appl. Phys.* **2017**, *122*, 143302. [[CrossRef](#)]
- Li, Y.; Zhang, X.; Xiao, S.; Chen, Q.; Wang, D. Decomposition characteristics of $C_5F_{10}O$ /air mixture as substitutes for SF_6 to reduce global warming. *J. Fluor. Chem.* **2018**, *208*, 65–72. [[CrossRef](#)]
- Deng, Y.; Chen, L.; Ma, Y.; Wang, D.; Zhao, S.; Xiao, D. Calculation and analysis of the thermophysical properties of $C_5F_{10}O-N_2$ mixtures. *AIP Adv.* **2019**, *9*, 105019. [[CrossRef](#)]
- Yoon, J.-H.; Ahn, H.-S.; Choi, J.; Oh, I.-S. An estimation technology of temperature rise in GIS bus bar using three-dimensional coupled-field multiphysics. In Proceedings of the Conference Record of the 2008 IEEE International Symposium on Electrical Insulation, Vancouver, BC, Canada, 9–12 June 2008; pp. 432–436.

18. Li, Y.; Zhang, X.; Li, X.; Cui, Z.; Xiao, H. Detection of ozone and nitric oxide in decomposition products of air-insulated switchgear using ultraviolet differential optical absorption spectroscopy (UV-DOAS). *Appl. Spectrosc.* **2018**, *72*, 1244–1251. [[CrossRef](#)] [[PubMed](#)]
19. Dervos, C.T.; Vassiliou, P.; Mergos, J.A. Thermal stability of SF₆ associated with metallic conductors incorporated in gas insulated switchgear power substations. *J. Phys. D Appl. Phys.* **2007**, *40*, 6942–6952. [[CrossRef](#)]
20. Li, Y.; Zhang, X.; Li, Y.; Wei, Z.; Wang, Y.; Ye, F.; Xiao, S. Effect of oxygen on power frequency breakdown characteristics and decomposition properties of C₅-PFK/CO₂ gas mixture. *IEEE Trans. Dielectr. Electr. Insul.* **2021**.
21. Hyrenbach, M.; Hintzen, T.; Müller, P.; Owens, J. Alternative gas insulation in medium-voltage switchgear. In Proceedings of the 23rd International Conference on Electricity Distribution, Lyon, France, 15–18 June 2015; pp. 15–18.
22. Miranda, F.M.; Miranda, F.M.; Caporali, S. SERS and DFT study of copper surfaces coated with corrosion inhibitor. *Beilstein J. Nanotechnol.* **2014**, *5*, 2489–2497. [[CrossRef](#)]
23. Li, Y.; Zhang, X.; Tian, S.; Xiao, S.; Chen, Q.; Chen, D.; Cui, Z.; Tang, J. Insight into the compatibility between C₆F₁₂O and metal materials: Experiment and theory. *IEEE Access* **2018**, *6*, 58154–58160. [[CrossRef](#)]
24. Wang, Y.; Lü, Y.; Zhan, W.; Xie, Z.; Kuang, Q.; Zheng, L. Synthesis of porous Cu₂O/CuO cages using Cu-based metal–organic frameworks as templates and their gas-sensing properties. *J. Mater. Chem. A* **2015**, *3*, 12796–12803. [[CrossRef](#)]
25. Zeng, J.; Zhuang, J.; He, T.; Chen, Q.; Liu, Y. Microstructure and dielectric response of Mg doped Cu₃Ti₂Ta₂O₁₂ ceramics. *J. Mater. Sci. Mater. Electron.* **2018**, *30*, 2652–2658. [[CrossRef](#)]
26. Delley, B. From molecules to solids with the DMol₃ approach. *J. Chem. Phys.* **2000**, *113*, 7756–7764. [[CrossRef](#)]
27. Zhang, X.; Li, Y.; Chen, D.; Xiao, S.; Tian, S.; Tang, J.; Wang, D. Dissociative adsorption of environment-friendly insulating medium C₃F₇CN on Cu(111) and Al(111) surface: A theoretical evaluation. *Appl. Surf. Sci.* **2018**, *434*, 549–560. [[CrossRef](#)]
28. Zhang, R.; Peng, M.; Duan, T.; Wang, B. Insight into size dependence of C₂ oxygenate synthesis from syngas on Cu cluster: The effect of cluster size on the selectivity. *Appl. Surf. Sci.* **2017**, *407*, 282–296. [[CrossRef](#)]
29. Özçelik, S.; Güvenç, Z.B. Structures and melting of Cu_n (n = 13, 14, 19, 55, 56) clusters. *Surf. Sci.* **2003**, *532*, 312–316. [[CrossRef](#)]
30. Shin, K.; Kim, D.H.; Yeo, S.C.; Lee, H.M. Structural stability of AgCu bimetallic nanoparticles and their application as a catalyst: A DFT study. *Catal. Today* **2012**, *185*, 94–98. [[CrossRef](#)]
31. Govind, N.; Petersen, M.; Fitzgerald, G.; King-Smith, D.; Andzelm, J. A generalized synchronous transit method for transition state location. *Comput. Mater. Sci.* **2003**, *28*, 250–258. [[CrossRef](#)]
32. Halgren, T.A.; Lipscomb, W.N. The synchronous-transit method for determining reaction pathways and locating molecular transition states. *Chem. Phys. Lett.* **1977**, *49*, 225–232. [[CrossRef](#)]